LUND UNIVERSITY

Aerodynamic efficiency explains flapping strategies used by birds

Johansson, Christoffer

Published in:
Proceedings of the National Academy of Sciences

DOI:
10.1073/pnas.2410048121

2024

Document Version:
Peer reviewed version (aka post-print)

Citation for published version (APA):
Johansson, C. (2024). Aerodynamic efficiency explains flapping strategies used by birds. *Proceedings of the National Academy of Sciences*, *121*(46), Article e2410048121. https://doi.org/10.1073/pnas.2410048121

Total number of authors:
1

LUND UNIVERSITY

PO Box 117
221 00 Lund
+46 46-222 00 00

PNAS

Main Manuscript for

Aerodynamic efficiency explains flapping strategies used by birds.

L. Christoffer Johansson*

Dept. Biology

Lund University

Naturvetarvägen 6A

SE-223 62 Lund, Sweden

* L. Christoffer Johansson

Email: Christoffer.Johansson@biol.lu.se

Author Contributions: L.C.J. conceived the study, performed the experiments, analysis, drew the figures and wrote the paper.

Competing Interest Statement: The authors have no competing interests.

Classification: Biological Sciences/Evolution, Physical Sciences/Physics

Keywords: Animal flight, bird aerodynamics, flight efficiency, flapping wing, bio-hybrid robot

This PDF file includes:

Main Text
Figures 1 to 4

Abstract

A faster cruising speed increases drag and thereby the thrust (*T*) needed to fly, while weight and lift (*L*) requirement remains constant. Birds can adjust their wingbeat in multiple ways to accommodate this change in aerodynamic force, but the relative costs of different strategies remain largely unknown. To evaluate the efficiency of several kinematic strategies, I used a robotic wing (Ajanic et al., 2023(1)) and quantitative flow measurements. I found that, among the tested strategies, changing the mean wingbeat elevation provides the most efficient solution to changing *T*/*L*, offering insight into why birds tend to beat their wings with a greater ventral than dorsal excursion. I also found that although propulsive efficiency (η_p) may peak at a Strouhal number (*St*, measure of relative flapping speed) near 0.3, the overall efficiency of generating force decreases with *St*. This challenges the expectance of a specific optimal *St* for flapping flight and instead suggest the chosen *St* depends on *T*/*L*. This may explain variation in preferred *St* among birds and why bats prefer flying at higher *St* than birds (Taylor et al., 2003(2)), since their body shape imposes relatively higher thrust requirements (Muijres et al., 2012(3)). In addition to explaining flapping strategies used by birds, my results suggest alternative, efficient, flapping motions for drones to explore aiming to extend their flight range.

Significance Statement

This research significantly advances our understanding of avian flight by revealing that an efficient kinematic strategy for birds is to flap their wings with a greater ventral than dorsal excursion. This strategy, overlooked previously, efficiently increases thrust and may have shaped the function of the flight apparatus. The study also challenges the notion that optimal flight and swimming are similar and should use a similar relative flapping velocities, highlighting fundamental differences in the selective pressures acting on these animals. Additionally, the findings offer exciting avenues for bio-inspired engineering, where understanding why birds use specific wing kinematics, as provided by this study, could significantly extend the flight range of flapping drones, addressing a main limitation in their design.

Main Text

Introduction

Birds, unlike airplanes, use their wings for both weight support and thrust generation simultaneously(4, 5). This is achieved by flapping the wings - tilting the aerodynamic force forwards(4, 5). In cruising flight, flying faster increases the drag and thereby the required thrust, while the lift needed to counter the weight and stay aloft remains constant(4, 5). To achieve the necessary change in thrust to lift ratio, birds can alter the aerodynamic properties of their wings - through adjusting the shape of the wings or the angle with which the air meets the wing – but they can also change their kinematics, i.e. how the wings are flapped. Indeed, we see that birds change their kinematics across speed(6–10), but also that they flap their wings in ways that currently lack a mechanistic explanation (e.g. flapping their wings with a mean elevation below the horizontal plane going through the shoulder joint). Since thrust and lift are inherently linked in flapping flight, the manner in which birds flap their wings likely affects the efficiency of generating both forces simultaneously, but not necessarily in the same way. This dynamic interplay provides an evolutionary selection pressure, driving birds toward optimal wing motions that achieve force balance as efficiently as possible. Despite the topic's relevance and our awareness that subtle changes in kinematics can have a large effect on force magnitude, vectoring and propulsive efficiency during flapping flight(1, 11–16), the topic has received relatively little attention. Understanding *why* birds flap their wings the way they do will help interpret the evolution of flight, the morphology and physiology of the flight apparatus and the diversity of flight styles found in nature(4, 5). However, our understanding of the relationship between kinematics and aerodynamic performance primarily relies on models that oversimplify wing kinematics(11, 12) or on correlative associations between kinematics and performance in flying birds(7, 8, 17–20). In these latter cases, untangling the effects of individual kinematic parameters becomes challenging, as birds often adjust multiple parameters simultaneously(6–8, 17–19). Consequently, we find ourselves lacking a mechanistic understanding of how specific wing motions and changes in motion across varying flight conditions impact performance and efficiency. To address this gap, we must explore alternative kinematic strategies to change *T*/*L* and assess their relative efficiency, which means going beyond studying birds.

Here I explore the kinematic parameter space of variables known to change with flight speed (U_∞) in birds(6–8, 10, 17–19, 21). I use a hybrid robotic wing(1) mounted in a wind tunnel(22) (Fig. 1c), and estimate the aerodynamic forces (Fig. 1d) and power (*P*) from the airflow measured behind the wing using particle image velocimetry (PIV)(19, 23). The wing is set to flap in a way resembling the flight of a jackdaw (Supplemental Figs 1 and 2) and is then adjusted to test three different scenarios, while maintaining wing shape and the angle relative to the flow between scenarios. In the first case, I compare the effects of adjusting the wingbeat amplitude (*A*) and frequency (*f*), as captured in the Strouhal number ($St = fA_{\mathrm{vert}}/U_\infty$, where A_{vert} is the tip-to-tip vertical excursion of the wing tip), when using a more realistic wing motion than previously used (e.g. (24–26)). In the second case I explore effects of adjusting the mean wing elevation (*MWE* = elevation - depression, Fig. 1a) during a wingbeat and finally I test the effects of adjusting downstroke ratio (*dsr*, the relative duration of the downstroke during a wingbeat, Fig. 1a) and the stroke plane angle (*SPA*, the direction the wing is flapped relative to the vertical). All the kinematic changes in each of these three scenarios have the potential to change *T*/*L* (Fig. 1b), but how they differ in efficiency is not known.

Results and discussion

One strategy to increase *T*/*L* is to increase the relative flapping velocity of the wing, by changing either A_{ang} (angular amplitude) or *f* (Fig. 1), and thereby tilt the aerodynamic force forwards(5). I found that both increasing A_{ang} and *f* (in effect increasing *St* when other parameters are kept constant) resulted in increased *T*/*L*, as expected (Fig. 2a & 3a, $p<0.0001$ in both cases). When comparing different measures of efficiency, I found that increasing *St*, within the range tested here, resulted in different trends for propulsive efficiency (η_p, see material and methods for definitions), cost of transport (COT) and power factor (PF). η_p increased with increasing *St* (Fig. 2d, $p<0.0001$), within the measured range, and the curve suggest a peak η_p near *St* = 0.3. COT increased with *St* (Fig. 2c, k = 2.07, $p<0.0001$), while PF (Supplemental Fig. S3c, $p<0.0001$) decreased, which both suggest that the efficiency of generating *L* and F_{use} (magnitude of the vector sum of *T* and *L*) decreases with increasing *St*, at least within the measurement range. Together, the results suggest that the optimum *St* will either be the lowest possible to achieve force balance or depend on the relative cost of generating *T* and *L*. A high relative *T* demand will favor a high η_p and result in a relatively high optimal *St*, while a low relative *T* demand will favor a low COT and thus a low optimal *St*.

Two decades ago, Taylor et al.(2) demonstrated that flying animals exhibit a preference to flap their wings within a *St* range of 0.2-0.4. This range has been associated with high η_p, around an optimal at *St* = 0.3, in heaving plates (e.g. (27)) and swimming animals(28), which suggested flying animals also optimized η_p. However, the goal of swimming (producing *T*) is not the same as for flying (producing *T and L*) nor is the motion of a tail fin (uniform along the span) and wing (pivoting around the base) the same. Consequently, it is not obvious why the optimal *St* should be consistent between swimming and flying. To date, as far as I know, no satisfactory explanation for the rather large observed variation (a factor two) in preferred *St* among flying animals(2) has been offered. Indeed, my results imply that a single optimal *St* for flapping flight may not exist. Instead, I propose that the chosen *St* should depend on the *T*/*L* and consequently that *St* alone has limited ability as predictor of optimal behavior in flying animals. I note that, in addition to variation in preferred *St* within clades (e.g. birds, bats and insects), the preferred *St* of flying bats tend to be higher than that of birds(2), which is consistent with bats having higher body drag(29, 30) and thus higher *T*/*L* demand than birds(3). This supports my argument that flapping flight differs in crucial perspectives from swimming and that we may expect higher variation in preferred *St* among flying compared to swimming animals since optimizing efficiency of *T* and *L* production may not require the same kinematics.

In my second scenario I tested an alternative strategy to change *T*/*L* that, as far as I know, has not previously been recognized: to change the mean wing elevation. When changing *MWE,* while maintaining *f* and A_{ang}, the wing continues to sweep through the same amount of air, at the same speed, and is expected to generate the same *T*. However, the resultant force of each wing tilts sideways, hence reducing *L* (Fig. 1b). The power required to generate the force is not expected to change, thus affecting efficiency relatively little. My results agreed with predictions for *T*/*L* (Fig. 3a, k = -0.0027, $p<0.0001$) and C_L (Fig. 3b, k = 0.0023, $p<0.0002$), but instead of constant thrust coefficient (C_T) I found an increase of C_T (Fig. 3b, k = -0.0019, $p<0.0001$) with decreasing *MWE*.

One potential explanation for the latter is that the tunnel wall acts as an aerodynamic mirror(31, 32). The wing then interacts with its mirror wing, causing a wing-wing interaction(33), enhancing T at the end of the downstroke. Such a wing-wing interaction is similar to the ground effect(34, 35) and has previously been suggested to help birds stay aloft during hovering flight(36). In addition to finding that C_T increased the smaller the angle between the wing and its mirror wing was, I found that T increased during the end of the downstroke with decreasing *MWE* (Supplemental Fig. S4), supporting this interpretation. When I compared the efficiency of the different strategies, changing f or A_{ang} vs changing *MWE*, I found that for positive T/L the *MWE* strategy had a lower increase in COT (T/L*Strategy, $p<0.0001$) and a higher increase in PF (Supplemental Fig. S3, T/L*Strategy, non-overlapping 95% CI). The propulsive efficiency, η_p, of the *MWE* strategy did not differ from the zero-*MWE* strategy (overlapping 95% confidence interval) relative to T/L (Fig. 3d) but resulted in higher η_p for a given *St* (excluded 95% CI in Fig. 2d). However, the *PF* was lower and had lower slope for the *MWE* strategy compared to the zero-*MWE* strategy when comparing across *St* (Supplemental Fig. S3c, *MWE* $p<0.0001$, *St* * *MWE* $p<0.0001$). These latter results may be caused by the definition of *St* (see below). An additional benefit of the *MWE* strategy was that T/L increased partly due to a decrease in C_L, which is needed to match weight support when flying faster ($L \propto C_L U_\infty^2$). If the increased T/L is instead achieved by only increasing C_T the animal would have to adjust its wingbeat to reduce L to maintain force balance at higher speeds. There are few, if any, studies available showing if birds adjust *MWE* across speeds, but there are several papers, from different species, showing that the mean wing elevation is below zero in birds(6–8, 37) (and bats, (38–41)) and my findings provide a plausible explanation for why. Exploring how *MWE* can benefit a wing-wing interaction in forward flight using different kinematic condition than studied here should thus provide exciting avenues for future research.

A consequence of using a subzero *MWE* with constant A_{ang} and f is that although the wing sweeps through the same amount of air at the same speed and aerodynamically should behave the same as when flapped symmetrically above and below the horizontal plane, the *St* changes. The reason is that *St* is defined using A_{vert}, which is related to the sine of the elevation and depression angles (above and below the horizontal plane, respectively). Flapping with the same A_{ang} thus results in a lower A_{vert} when *MWE* differs from zero compared to when it is zero (Fig. 3b). The effect can be rather substantial. With an A_{ang} of 75 degrees and a *MWE* of -25 degrees *St* is 10 % lower than if the wing is flapped symmetrically around the horizon (Fig. 3b). Birds fly at *St* close to, or even below, the lower limit of the optimal *St* range(2) for propulsive efficiency (0.2-0.4), which could be explained by birds tending to flap their wings with a subzero *MWE*(6–8, 37). However, since bats also tend to flap their wings with a negative *MWE*$^{(\mathrm{e.g.}}$ (38–41)$^{)}$ and still flap at higher *St* than birds this effect would not necessarily explain the differences between birds and bats in preferred *St* discussed earlier and a proper test of the effect of *MWE* on birds and bats is required. Since *St* is intended to capture the transverse motion of the wing, or fin, in relation to the forward flight direction, I conclude that the current definition fails to do so when the *MWE* is subzero (or above zero). I therefore suggest that instead of using A_{vert} to calculate *St* we should use the distance the wing tip moves transverse to the direction of flight.

In my final set of experiments, I varied downstroke ratio (*dsr*) and stroke plane angle (*SPA*)(Fig. 1a), which both affect the path the wing moves through the air and the relation between the vertical and horizontal velocity of the wing (Fig. 1b). A higher *dsr* results in a lower flapping velocity and a shallower path of the wing during the downstroke than with a lower *dsr,* predicting the resultant force to be more upwards directed. The same prediction is generated by increasing the *SPA*. It should be noted that the exact effects of these changes may depend on the effect of the upstroke, which relies on how much the wing can retract. The robotic wing has limited ability to retract, and it will be of great interest to further explore these effects in different bird species where the upstroke is used to different degrees for force production. As expected, both the *dsr* and *SPA* strategies affected the T/L and in general I found that tilting the *SPA* reduced the T/L ($p<0.0001$), following predictions, while deviating from a *dsr* of 0.5-0.55 instead increased T/L (Fig. 4a, $dsr^2>0$, $p<0.0001$). For increased *dsr*, this latter result is likely a consequence of an increased vertical speed during the upstroke resulting in the outer part of the wing generating more T (Fig. 4b), since I at the same time found a higher C_L with increased *dsr* ($k=1.20$, $p<0.0001$). The latter was according to expectations from a shallower and longer duration downstroke. A decreased *dsr*, on the other hand, increases the *T* during the downstroke by tilting the downstroke aerodynamic force forwards. Increasing *SPA*, resulted in increased COT (Fig. 4c, $p<0.0001$) and decreased PF (Supplemental Fig. S3e, $p<0.0001$) compared to a vertical stroke plane, while *dsr* did not have any noticeable effect on COT (Fig. 4c, $p=0.45$) or PF (Supplemental Fig. S3e, $p=0.64$). dsr did not seem to influence η_p (Fig. 4d, dsr $p=0.16$ and dsr * *T*/*L* $p=0.11$), but for *SPA* there was a lower intercept the higher the SPA ($p<0.0028$) and a lower increase in efficiency the higher the SPA ($p<0.0001$). Compared to the strategy of changing only *f* and *A*, the *SPA* and *dsr* strategies resulted in a higher intercept ($p<0.0001$), but a lower slope for η_p across *T*/*L* ($p<0.0001$) resulting in lower η_p for positive *T*/*L*. I conclude that one probable reason birds and other animals increase *SPA* when flying slower$^{e.g.}$ (7, 19, 21) is to reduce the thrust while maintaining lift (Fig. 4 b) i.e. to be able to achieve force balance (as previously suggested by other studies e.g. (1, 16, 21)) and not generate too much thrust resulting in an acceleration, since this strategy comes with an increase in COT and a reduction in η_p. Changing *dsr*, as many birds do(6–9), may, on the other hand, be a flexible solution where changing the relative time of the downstoke increases *T*/*L* without apparent effects on either COT nor η_p. The same change in *dsr* had a larger effect on *T*/*L* when decreasing *dsr* compared to increasing it (Fig. 4a), suggesting that it may be more effective for animals to decrease *dsr* to increase *T*/*L*, which also seems to be preferred by birds(6–9). A small change in the contraction velocity of the muscles, which a change in *dsr* implies, may also maintain muscle efficiency and thereby the physiological cost of accommodating the change(4).

Conclusion

My study addresses a fundamental problem of flight with flapping wings: how to best deal with changes in the relative need for thrust and lift. My findings, based on systematic tests of different kinematics using a robotic wing, provide explanations for behaviors seen in real birds that have previously been ignored. Birds use a subzero mean wing elevation, which my results show is an efficient strategy to change the thrust to lift ratio (Fig. 3a). Also changing the downstroke ratio, as birds do, provides a flexible way to change the thrust to lift ratio without negative effects on efficiency. The results also provide an explanation for the systematic, unexpected, variation seen in preferred Strouhal number among flying animals(2). The fact that swimming animals seem to optimize propulsive efficiency by controlling their St has inspired the idea of a universal optimal St also in flying animals, based on propulsive efficiency, but my findings provide evidence this may not be the case. Instead, the selected St during flight should depend on the thrust to lift ratio (Fig. 2). The reasoning behind this stems from the fundamental difference between the goal of swimming – producing thrust – and the goal of flying – producing both thrust and lift. Or put in a different way, that the produced force is aligned with the direction of travel in swimming, but not in flight. That said, there is a large variation in shape and flight style among flying animals and how these factors interact with the kinematic factors proposed here to determine the St selected by animals during cruising flight provides exciting prospects for future studies. Taken together, my findings should not only help to better understand the kinematics selected by flying animals, but also provide alternatives for efficient flapping kinematics to be explored by flapping micro air vehicles(42).

Materials and Methods

For this study I used an updated version of the hybrid robotic wing previously described in Ajanic et al. (1). The robot is based on a jackdaw (wing length 0.33 m) with a skeleton consisting of 3D printed “bones” and has a wing partly built by real flight feathers and partly by carbon fiber plates and silicone membranes (Fig. 1c). The robot is capable of independently controlling the angular elevation of the wing above (max 90 degrees) and angular depression of the wing below (max 90 degrees) the horizontal plane through the flapping axis, the wingbeat frequency (*f*, in the range 0-15 Hz) and the pitch angle (γ, varying ±40 degrees). These factors can be controlled as continuous functions over time and essentially take any shape allowed by motor accelerations. Here I used this flexibility to control the mean wing elevation (*MWE*, elevation-depression angles), the downstroke ratio (*dsr*, which can be set between 0.2-0.8) and the angle of attack (α). In addition, the robot is mounted on a circular plate in the wind tunnel wall that allows setting the stroke plane angle (*SPA*, can be set to 0-40 degrees) by rotating the entire robot. The robot also has a wing folding mechanism, here allowing for a wing retraction during the upstroke (with a minimum span ratio of 0.7), by sweeping the hand wing and folding the arm wing. The robot is controlled using a custom software via a microcontroller (Nucleo-144, STM32F429ZIT6, STMicroelectronics, USA). Compared to the original version of the robot(1), two changes have been made. First, the motor controlling the wing folding has been replaced with a ClearPath-SDSK (Teknic, Victor, USA). Second, the software limitation of a maximum *f* has been changed from 5 Hz to 15 Hz. To accommodate these changes the control software has been updated.

I ran three different sets of experiments, one investigating the effect of Strouhal number (*St*), one investigating the effect of *MWE* and one looking at the effects of changing *dsr* and *SPA*. All experiments were conducted at a tunnel speed of U_∞ = 8 m/s. For each kinematic condition I took three measurements. The wing motion was stopped between each measurement and subsequently started again. This provides unique starting conditions for the wing for each sequence, and I therefore considered the measurements to be statistically independent.

Prior to the experiments I conducted measurements of the wing extended and at zero flapping angle across a range of pitch angles to determine the zero-lift pitch angle. This angle was then used as a reference angle to calculate the pitch angle needed to generate the desired *α* of the wing. For all experiments the wing was then flapped, with each half stroke (downstroke or upstroke) following a sinusoidal curve for the flapping angle with the angular speed determined by the A_{ang}, *f* and *dsr*. The α was set to follow a sinusoidal curve with a peak value of 18 degrees during the downstroke and 3 degrees during the upstroke. At the turning points the wing was set to have an α of 2 degrees, by adding 2 degrees to the angle of attack throughout the wingbeat. The α was determined at a position mid wing, taking into account the wing retraction during the upstroke and the flapping velocity and direction. The *MWE* was set by independently controlling the maximum elevation and depression angle of the wing. Wing length (*b*(*t*)) was controlled to have its maximum during the downstroke and minimum during the upstroke. To allow the change in wing length to occur smoothly and distributed in time around the transitions between downstroke and upstroke I started the retraction of the wing 25% of the duration of the upstroke plus 3% of the stroke duration before the start of the upstroke and finish the extension of the wing 25% of the duration of the upstroke minus 3% of the stroke duration into the downstroke. The retraction and extension of the wing followed a sinusoidal curve to generate a smooth motion (Supplemental material, Fig. S1).

For measurements of the aerodynamic performance of the robot I used stereo particle image velocimetry (sPIV) in a plane perpendicular to the freestream flow of the Lund University wind tunnel(22). The sPIV system (Lavision, Göttingen, Germany) includes a dual pulse laser (LDY304PIV laser, Litron Lasers, Rugby, England), operated at f_L=720 Hz, four high speed cameras (Photron Nova R2, Photron Deutschland GmbH, Reutlingen, Germany) and acquisition and analysis software (Davis 10.2.1, Lavision, Göttingen, Germany). The cameras were set up in a side-by-side configuration, where two cameras viewed the right side of the tunnel (upper part of the wingbeat) and two cameras viewed the left side (the lower part of the wingbeat), similar to Ajanic et al.(1). The analysis settings were; pre-processing with a subtract sliding background of length 32, followed by a vector calculation with an initial box size of 64x64 and a final box size of 32x32, with 50% overlap. The final vector field, with a vector spacing of 3.8 mm (~2.6 vectors/cm), was subjected to a vector validation of strength 2. To remove erroneous vectors and noise I ran an anisotropic denoising with strength 2.5 using a 9x9 kernel and a fixed uncertainty of 0.1. As a final step I ran “Fill small gaps in the vector field” process with two passes. The resulting vector fields party overlapped and were merged into a single vector field rotated to be aligned with normal flight conditions i.e. downwards aligned with gravity. The final vector field was approximately maximum 600 mm in the spanwise direction and 780 mm in the vertical direction, with a somewhat irregular shape.

The vector fields were analyzed using custom written software in Matlab R2022a (Mathworks Inc.). The data were masked to remove erroneous vectors at the edge of the vector field and mirrored in the sagittal plane of the robot, to generate a wake representing both wings of a bird. Mirroring the vector field is motivated by the wind tunnel wall acting as an aerodynamic mirror ((31–33, 35)), making it possible to study wing-wing interactions using a single wing (33). This procedure ignores effects of the boundary layer, but given that the boundary layer in the current tunnel is thin (34) and that all measurements are performed at the same speed I consider these effects to be small. To remove any effects of calibration errors or systematic variation in the background flow I estimated the average flow field of the static wing at zero-lift angle of attack and removed the wake of the wing by setting a threshold to the free-stream flow. I then fitted a plane to the velocity component in the freestream direction using the fit function in Matlab (with settings 'poly11','robust','bisquare' and 'Weights', where the weights were the inverse of the product of the standard deviations for each velocity component). I subtracted the systematic variation in background flow and then estimated the mean of the background flow (U_∞) before proceeding with the analysis. The mean background flow was determined as the freestream speed that generated the lowest mean square of the residuals when subtracting the speed from the measured streamwise velocity in an area of the measurements not affected by the wake of the wing. I stacked the vector fields in the streamwise direction with a spacing of U_∞/f_L and estimated the vorticity (ω, a measure of the rotation of the flow) as the curl of the flow velocities in the volume.

For the force calculations I used a masking procedure based on the total vorticity, previously described in(43) to isolate the wake structures and reduce the effect of noise in the flow.

The weight support or lift (L) was calculated according to,

$$L = \rho U_\infty \iint_{wake\ area} (y - y_0) \cdot \omega_x(y,z)\, dydz$$

where ρ is the air density, y is the spanwise position, y_0 the spanwise position of the center of the body and ω_x is the vorticity along the freestream axis.

I estimated the thrust (T) as the time derivative of the impulse(44) in the direction of flight as,

$$T = \frac{1}{2}\rho U_\infty \iint_{wake\ area} (y - y_0) \cdot \omega_z(y,z) - (z - z_0) \cdot \omega_y(y,z)\, dydz$$

where ω_z is the vorticity along the vertical axis, ω_y is the vorticity along the spanwise axis, z the vertical position and z_0 the vertical position of the center of the body.

For the comparisons in this paper, I used the time-averaged force over three wingbeats. To evaluate the performance of the different kinematic conditions I calculated several key parameters. The direction of the resultant force was determined as the average thrust to average lift ratio (*T*/*L*) and the ability to generate force was determined by estimating the force coefficients,

$$C_L = \frac{L}{\mathrm{qS}}$$
$$C_T = \frac{T}{\mathrm{qS}}$$

where q is the dynamic pressure ($\mathrm{q}=\frac{1}{2}\rho \mathrm{U}_\infty^2$) and S is the wing area.

I also made an estimate of the relative useful force (F_{use}) as the magnitude of the vector sum of T and L. Since T was sometimes negative, which does not constitute a useful force, I subtracted the minimum T (based on all sequences) from all the measurements before estimating F_{use}. As with T and L I normalized F_{use} according to,

$$C_{Fuse} = \frac{F_{use}}{\mathrm{qS}}$$

To get a measure of the cost of generating the forces I estimated the kinetic energy in the wake(19, 23). For this purpose, I used the masked vorticity field (see above) to estimate the flow using the Helmholtz-Hedge decomposition and extend it beyond the dimensions of the wind tunnel (here to a size of 2.4x2.4 m cross section)(19, 23). Due to the flow field being reconstructed from the vorticity based on the stacked 2D-slices of the flow, velocity at the edges of the volume did not always become zero. I therefore subtracted the mean streamwise velocity at the edges of the volume before calculating the kinetic energy. The kinetic energy was estimated according to,

$$E = \frac{1}{2}\rho \iiint_{Wake\ volume} (u^2 + v^2 + w^2) \cdot \left(1 + \frac{u}{U_\infty}\right) dx\, dy\, dz,$$

where u, v, w are the induced velocities in x, y, z, respectively. From the kinetic energy I estimated the power by dividing with the number of wingbeats (N_{wb}=3) and multiplying with the wingbeat frequency (*f*). Since the net thrust does not necessarily sum to zero in this setup I added TU_∞ to the estimate the total power (P), which can be seen through eq 34 in (45) looking only at the work rate through the Treftz-plane and assuming zero pressure work.

$$P = \frac{E}{N_{wb}} f + TU_\infty,$$

I then normalized the power by calculating the power coefficient (C_P) as,

$$C_P = \frac{P}{qSU_\infty}$$

Since the force generation differs between the different kinematic settings, I estimated several performance parameters to allow for a comparison between the cases. A traditional measure of performance is the cost of transport (COT), defined as the energy required to transport a unit of weight a unit of distance. By equating the weight with the lift generated by the wing I estimated COT as,

$$COT = \frac{P}{LU_\infty}$$

The propulsive efficiency (η_P) as,

$$\eta_P = \frac{C_T}{C_P}$$

, the power factor (PF) as

$$PF = \frac{C_{Fuse}^{1.5}}{C_P}$$

and the $F_{use}/\bar{\varepsilon}$ where $\bar{\varepsilon}$ is the mean enstrophy estimated as

$$\bar{\varepsilon} = \mathrm{mean}(|\omega|^2)$$

Each of these factors represents different aspects of efficiency, where COT is a measure of the relative cost of generating L (weight support) while the propulsive efficiency relates to the efficiency of thrust production. The power factor originates from the actuator disk model and the fact that force is proportional to the induced velocity squared, while power is proportional to the induced velocity cubed. Enstrophy has previously been shown to scale with power(46) and $F_{use}/\bar{\varepsilon}$ is thus a measure similar to the milage of a car. Since ε is estimated from ω and not the velocities the wake structures have a relatively larger influence on the results and the extension of the wake as done for the kinetic energy estimate is not needed.

To compare the outcomes of the different kinematic strategies I performed general linear models in JMP Pro 15.0.0 (SAS Institute Inc., Cary, USA). For the *T*/*L* and C_T data I tested against a second order polynomial for the relation with *dsr*, but in the other cases I used a linear function. For the η_P data I performed a Yeo-Johnson transformation(47) prior to the analysis. The l-coefficient was chosen to get the most linear data based on the loglikelihood of a fitted linear model in Matlab. l for the data in Fig. 2d was 2.8, in Fig. 3d 3.8 and in Fig. 4d it was 4.4.

Acknowledgments

I am grateful to the work of Kristoffer Westring for updating the robot and to Arne Hegerman for providing replacement feathers. The research was funded by the Crafoord foundation (20170584) and the Swedish Research Council (2017-03890 and 2022-02850) to L.C.J.. The PIV equipment was financed by an infrastructure grant from Lund University (https://www.lu.se/) to Anders Hedenström, Per Henningsson and L.C.J..

References

1. E. Ajanic, A. Paolini, C. Coster, D. Floreano, C. Johansson, Robotic Avian Wing Explains Aerodynamic Advantages of Wing Folding and Stroke Tilting in Flapping Flight. *Advanced Intelligent Systems* **5**, 2200148 (2023).

2. G. K. Taylor, R. L. Nudds, A. L. Thomas, Flying and swimming animals cruise at a Strouhal number tuned for high power efficiency. *Nature* **425**, 707–711 (2003).

3. F. T. Muijres, L. C. Johansson, M. S. Bowlin, Y. Winter, A. Hedenström, Comparing Aerodynamic Efficiency in Birds and Bats Suggests Better Flight Performance in Birds. *PLoS ONE* **7**, e37335 (2012).

4. C. J. Pennycuick, *Modelling the flying bird.* (Elsevier, 2008).

5. U. M. Norberg, *Vertebrate flight. Mechanics, Physiology, Morphology, Ecology and Evolution.* (Springer Verlag, 1990).

6. K. J. Park, M. Rosén, A. Hedenström, Flight kinematics of the barn swallow (*Hirundo rustica*) over a wide range of speeds in a wind tunnel. *Journal of Experimental Biology* **204**, 2741–2750 (2001).

7. M. Rosén, G. R. Spedding, A. Hedenström, Wake structure and wingbeat kinematics of a house-martin *Delichon urbica*. *J. R. Soc. Interface.* **4**, 659–668 (2007).

8. M. Rosén, G. R. Spedding, A. Hedenström, The relationship between wingbeat kinematics and vortex wake of a thrush nightingale. *J. Exp. Biol.* **207**, 4255–4268 (2004).

9. T. L. Hedrick, B. W. Tobalske, A. A. Biewener, How cockatiels (*Nymphicus hollandicus*) modulate pectoralis power output across flight speeds. *Journal of Experimental Biology* **206**, 1363–1378 (2003).

10. B. W. Tobalske, T. L. Hedrick, A. A. Biewener, Wing kinematics of avian flight across speeds. *Journal of Avian Biology* **34**, 177–184 (2003).

11. H. Salehipour, D. J. Willis, A coupled kinematics–energetics model for predicting energy efficient flapping flight. *Journal of Theoretical Biology* **318**, 173–196 (2013).

12. M. Klein Heerenbrink, L. C. Johansson, A. Hedenström, Power of the wingbeat: modelling the effects of flapping wings in vertebrate flight. *Proc. R. Soc. A.* **471**, 20140952 (2015).

13. S. S. Bhat, J. Zhao, J. Sheridan, K. Hourigan, M. C. Thompson, Effects of flapping-motion profiles on insect-wing aerodynamics. *J. Fluid Mech.* **884**, A8 (2020).

14. W. J. Maybury, F.-O. Lehmann, The fluid dynamics of flight control by kinematic phase lag variation between two robotic insect wings. *J. Exp. Biol.* **207**, 4707–4726 (2004).

15. G. Koekkoek, *et al.*, Stroke plane angle controls leading edge vortex in a bat-inspired flapper. *Comptes Rendus Mécanique* **340**, 95–106 (2012).

16. D. D. Chin, D. Lentink, Birds repurpose the role of drag and lift to take off and land. *Nat Commun* **10**, 5354 (2019).

17. P. Henningsson, G. R. Spedding, A. Hedenström, Vortex wake and flight kinematics of a swift in cruising flight in a wind tunnel. *Journal of Experimental Biology* **211**, 717–730 (2008).

18. F. T. Muijres, M. S. Bowlin, L. C. Johansson, A. Hedenström, Vortex wake, downwash distribution, aerodynamic performance and wingbeat kinematics in slow-flying pied flycatchers. *J. R. Soc. Interface.* **9**, 292–303 (2012).

19. L. C. Johansson, M. Maeda, P. Henningsson, A. Hedenström, Mechanical power curve measured in the wake of pied flycatchers indicates modulation of parasite power across flight speeds. *J. R. Soc. Interface.* **15**, 20170814 (2018).

20. A. Hedenström, M. Rosén, G. R. Spedding, Vortex wakes generated by robins *Erithacus rubecula* during free flight in a wind tunnel. *J. R. Soc. Interface.* **3**, 263–276 (2006).

21. B. W. Tobalske, *et al.*, Three-dimensional kinematics of hummingbird flight. *Journal of Experimental Biology* **210**, 2368–2382 (2007).

22. C. J. Pennycuick, T. Alerstam, A. Hedenström, A new low-turbulence wind tunnel for bird flight experiments at Lund University, Sweden. *J. Exp. Biol.* **200**, 1441–1449 (1997).

23. R. Von Busse, R. M. Waldman, S. M. Swartz, C. C. Voigt, K. S. Breuer, The aerodynamic cost of flight in the short-tailed fruit bat (*Carollia perspicillata*): comparing theory with measurement. *J. R. Soc. Interface.* **11**, 20140147 (2014).

24. T. Y. Hubel, C. Tropea, Experimental investigation of a flapping wing model. *Exp Fluids* **46**, 945–961 (2009).

25. A. Roshanbin, F. Abad, A. Preumont, Kinematic and Aerodynamic Enhancement of a Robotic Hummingbird. *AIAA Journal* **57**, 4599–4607 (2019).

26. A. K. Stowers, D. Lentink, Folding in and out: passive morphing in flapping wings. *Bioinspir Biomim* **10**, 025001 (2015).

27. J. M. Anderson, K. Streitlien, D. S. Barrett, M. S. Triantafyllou, Oscillating foils of high propulsive efficiency. *J. Fluid Mech.* **360**, 41–72 (1998).

28. M. S. Triantafyllou, G. S. Triantafyllou, D. K. P. Yue, Hydrodynamics of Fishlike Swimming. *Annual Review of Fluid Mechanics* **32**, 33–53 (2000).

29. J. D. Gardiner, G. Dimitriadis, W. I. Sellers, J. R. Codd, The aerodynamics of big ears in the brown long-eared bat Plecotus auritus. *Acta Chiropterologica* **10**, 313–321 (2008).

30. J. Håkansson, L. Jakobsen, A. Hedenström, L. C. Johansson, Body lift, drag and power are relatively higher in large-eared than in small-eared bat species. *J. R. Soc. Interface.* **14**, 20170455 (2017).

31. J. Lighthill, A simple fluid-flow model of ground effect on hovering. *J. Fluid Mech.* **93**, 781 (1979).

32. J. M. V. Rayner, On the aerodynamics of animal flight in ground effect. *Phil. Trans. R. Soc. Lond. B* **334**, 119–128 (1991).

33. M. Percin, Y. Hu, B. W. van Oudheusden, B. Remes, F. Scarano, Wing Flexibility Effects in Clap-and-Fling. *International Journal of Micro Air Vehicles* **3**, 217–227 (2011).

34. L. C. Johansson, L. Jakobsen, A. Hedenström, Flight in Ground Effect Dramatically Reduces Aerodynamic Costs in Bats. *Current Biology* **28**, 3502-3507.e4 (2018).

35. D. B. Quinn, G. V. Lauder, A. J. Smits, Flexible propulsors in ground effect. *Bioinspir. Biomim.* **9**, 036008 (2014).

36. Y.-H. Chang, S.-C. Ting, C.-C. Liu, J.-T. Yang, C.-Y. Soong, An unconventional mechanism of lift production during the downstroke in a hovering bird (Zosterops japonicus). *Exp Fluids* **51**, 1231–1243 (2011).

37. L. C. Johansson, A. Hedenström, The vortex wake of blackcaps (*Sylvia atricapilla* L.) measured using high-speed digital particle image velocimetry (DPIV). *Journal of Experimental Biology* **212**, 3365–3376 (2009).

38. R. Von Busse, A. Hedenström, Y. Winter, L. C. Johansson, Kinematics and wing shape across flight speed in the bat, *Leptonycteris yerbabuenae*. *Biology Open* **1**, 1226–1238 (2012).

39. M. Wolf, L. C. Johansson, R. Von Busse, Y. Winter, A. Hedenström, Kinematics of flight and the relationship to the vortex wake of a Pallas' long tongued bat (*Glossophaga soricina*). *Journal of Experimental Biology* **213**, 2142–2153 (2010).

40. T. Y. Hubel, N. I. Hristov, S. M. Swartz, K. S. Breuer, Changes in kinematics and aerodynamics over a range of speeds in *Tadarida brasiliensis* , the Brazilian free-tailed bat. *J. R. Soc. Interface.* **9**, 1120–1130 (2012).

41. T. Y. Hubel, D. K. Riskin, S. M. Swartz, K. S. Breuer, Wake structure and wing kinematics: the flight of the lesser dog-faced fruit bat, *Cynopterus brachyotis*. *Journal of Experimental Biology* **213**, 3427–3440 (2010).

42. J.-H. Han, Y.-J. Han, H.-H. Yang, S.-G. Lee, E.-H. Lee, A Review of Flapping Mechanisms for Avian-Inspired Flapping-Wing Air Vehicles. *Aerospace* **10**, 554 (2023).

43. L. C. Johansson, P. Henningsson, Butterflies fly using efficient propulsive clap mechanism owing to flexible wings. *J. R. Soc. Interface.* **18**, 20200854 (2021).

44. W. Tong, Y. Yang, S. Wang, Estimating thrust from shedding vortex surfaces in the wake of a flapping plate. *J. Fluid Mech.* **920**, A10 (2021).

45. M. Drela, Power Balance in Aerodynamic Flows. *AIAA Journal* **47**, 1761–1771 (2009).

46. E. Demirer, O. A. Oshinowo, A. Alexeev, Efficient aquatic locomotion using elastic propulsors with hybrid actuation. *Journal of Fluid Mechanics* **922**, A21 (2021).

47. I.-K. Yeo, R. A. Johnson, A New Family of Power Transformations to Improve Normality or Symmetry. *Biometrika* **87**, 954–959 (2000).

Figures and Tables

Figure 1. A robotic wing is used to control the flapping motion. a) The wing can separately set the elevation and depression angle to set the angular amplitude (A_{ang}) and change the mean wing elevation (*MWE*). The pitching angle can be adjusted as a continuous function over time to control the angle of attack (α). In addition, the wing can fold, and the stroke plane angle (*SPA*), the direction relative to the vertical that the wing is flapped, can be adjusted by rotating the circular plate that the robot is mounted on. The flapping frequency (f) can be set between 1 and 15 Hz and the motion adjusted as a continuous function over time, allowing control of the relative duration of the downstroke within the wingbeat (downstroke ratio, *dsr*). See Ajanic et al. (1) for details. **b)** Several kinematic changes relative to a symmetrical flapping (upper left) are expected to alter the direction of the force generated, as shown by the vector sum of thrust (T) and lift (L). Here changes in the direction of the force at mid downstroke, relative to the vector for symmetrical flapping (transparent in background) are shown while varying different kinematic parameters. Light blue shaded areas indicate upstroke. **c)** The hybrid robotic wing(1) mounted in the Lund University wind tunnel(22). **d)** A sample sequence of lift (L) and thrust (T) measured from the wake of the robotic wing during one wingbeat period. Curves show averages of three wingbeats.

Figure 2. Optimal Strouhal number (*St*) depends on flight demands. a) Increased *St* resulted in increased thrust to lift ratio (*T*/*L*) and a fixed *St* resulted in different *T*/*L* depending on the frequency-angular amplitude combination when the mean wing angle (*MWE*) is below zero. **b)** The same wing motion, i.e. *f* and A_{ang}, result in different *St* depending on the *MWE*, due to the effect of *MWE* on the vertical amplitude (A_{vert}) used in the *St* definition. This shows that the current definition of *St* is not suitable for flapping flight. **c)** and **d)** Within the range of *St* studied here, efficiency of lift production (low Cost Of Transport, COT) decreased with increasing *St* while the propulsive efficiency (η_P) increased, suggesting preferred *St* depends on the *T*/*L* required to fly. For a given *St*, η_P was higher when using a *MWE* of -15 degrees than when flapping with *MWE* of 0 degrees. Birds tend to fly at lower *St* than bats(2), as indicated by the images next to the *St* illustrations.

Figure 3. Mean wing elevation (*MWE*) can control thrust to lift ratio (*T*/*L*) and flight efficiency. a) Increased flapping frequency (*f*) and amplitude (A_{ang}) resulted in increased *T*/*L*, but so did lowering *MWE*. **b)** The increased *T*/*L* when lowering *MWE* is a result of a decreasing lift coefficient (C_L) and an increasing thrust coefficient (C_T). The latter is likely a result of increasing wing-wing interaction at the end of the downstroke. **c)** and **d)** When C_T is positive, decreasing *MWE* resulted in more efficient lift production (lower Cost Of Transport, COT) but not a higher propulsive efficiency (η_P) than when achieving the same *T*/*L* by increasing *f* or A_{ang}.

Figure 4. Downstroke ratio (*dsr*) and stroke plane angle (*SPA*) influence lift (*L*) and thrust (*T*). a) Deviating away from a *dsr* (the relative duration of the downstroke) of 0.5-0.55 increased *T*/*L*, while tilting the *SPA* reduced *T*/*L*. **b)** *SPA* had little influence on the lift coefficient (C_L) but reduced the trust coefficient (C_T). Increasing the *dsr* increased C_L, while deviating from a *dsr* of 0.5-0.55 increased C_T. **c)** The Cost Of Transport (COT) increased with increased *SPA* but did not vary with *dsr*. **d)** The propulsive efficiency (η_P) was negatively affected by increasing SPA, compared to the strategy of only changing *f* or *A*.

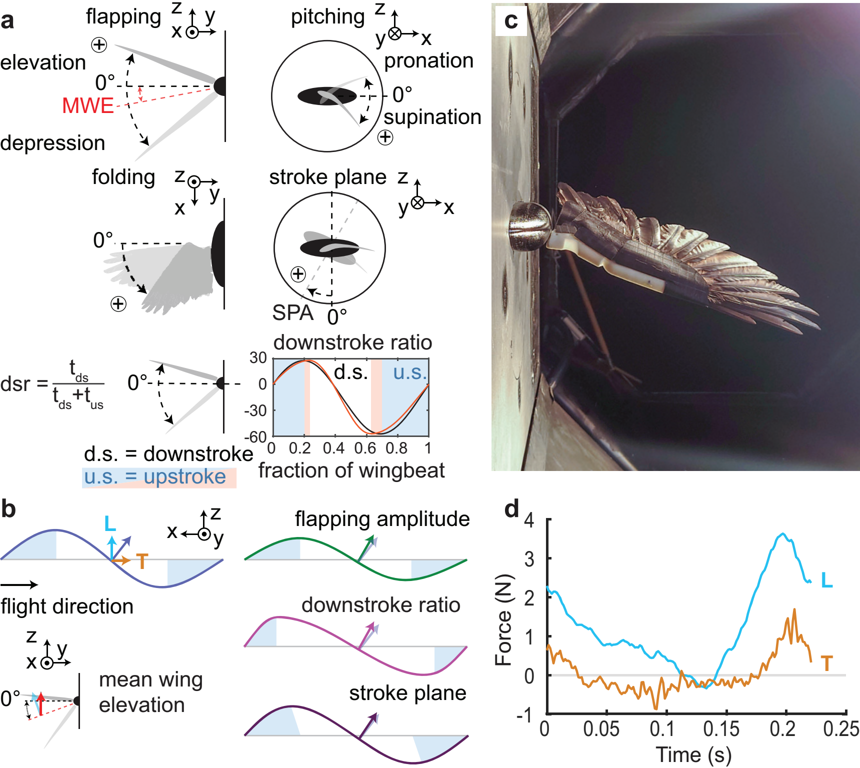
a
flapping
z y x
elevation
0°
MWE
depression
pitching
z y x
pronation
0°
supination
folding
z x y
0°
stroke plane
z y x
SPA
0°
dsr = $\frac{t_{ds}}{t_{ds}+t_{us}}$
0°
downstroke ratio
d.s.
u.s.
30
0
-30
-60
0
0.2
0.4
0.6
0.8
1
fraction of wingbeat
d.s. = downstroke
u.s. = upstroke
c
b
L
T
x z y
flight direction
z y x
0°
mean wing elevation
flapping amplitude
downstroke ratio
stroke plane
d
Force (N)
4
3
2
1
0
-1
0
0.05
0.1
0.15
0.2
0.25
Time (s)
L
T

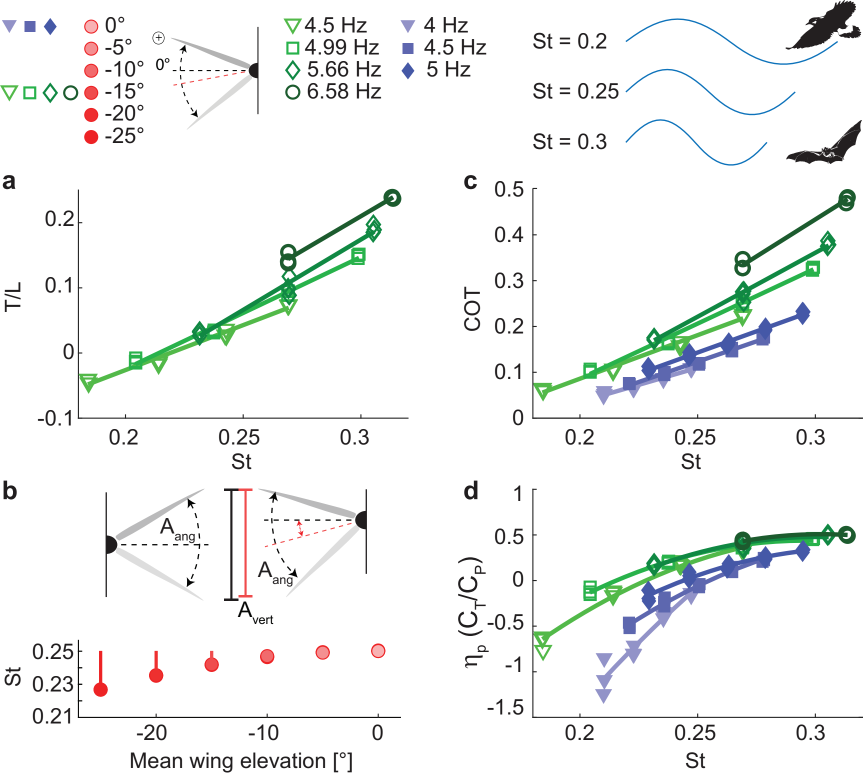
0°
-5°
-10°
-15°
-20°
-25°
⊕
0°
4.5 Hz
4.99 Hz
5.66 Hz
6.58 Hz
4 Hz
4.5 Hz
5 Hz
St = 0.2
St = 0.25
St = 0.3
a
T/L
0.2
0.1
0
-0.1
0.2
0.25
0.3
St
b
A_ang
A_ang
A_vert
St
0.25
0.23
0.21
-20
-10
0
Mean wing elevation [°]
c
COT
0.5
0.4
0.3
0.2
0.1
0
0.2
0.25
0.3
St
d
η_p (C_T/C_P)
1
0.5
0
-0.5
-1
-1.5
0.2
0.25
0.3
St

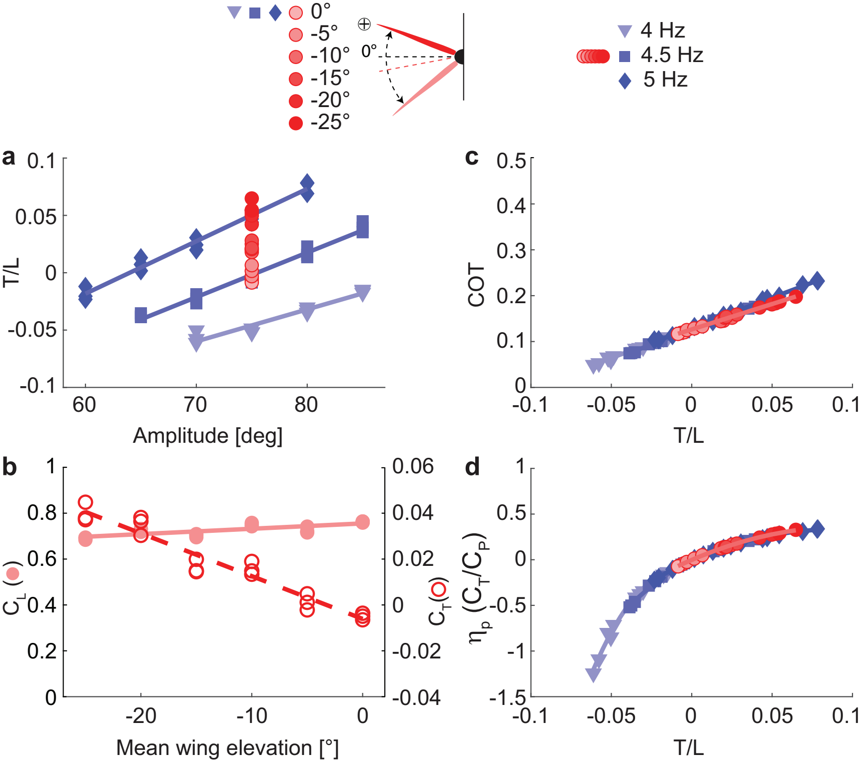
0°
-5°
-10°
-15°
-20°
-25°
⊕
0°
4 Hz
4.5 Hz
5 Hz
a
T/L
0.1
0.05
0
-0.05
-0.1
60
70
80
Amplitude [deg]
b
C_L (●)
C_T (○)
1
0.8
0.6
0.4
0.2
0
0.06
0.04
0.02
0
-0.02
-0.04
-20
-10
0
Mean wing elevation [°]
c
COT
0.5
0.4
0.3
0.2
0.1
0
-0.1
-0.05
0
0.05
0.1
T/L
d
η_p (C_T/C_P)
1
0.5
0
-0.5
-1
-1.5
-0.1
-0.05
0
0.05
0.1
T/L

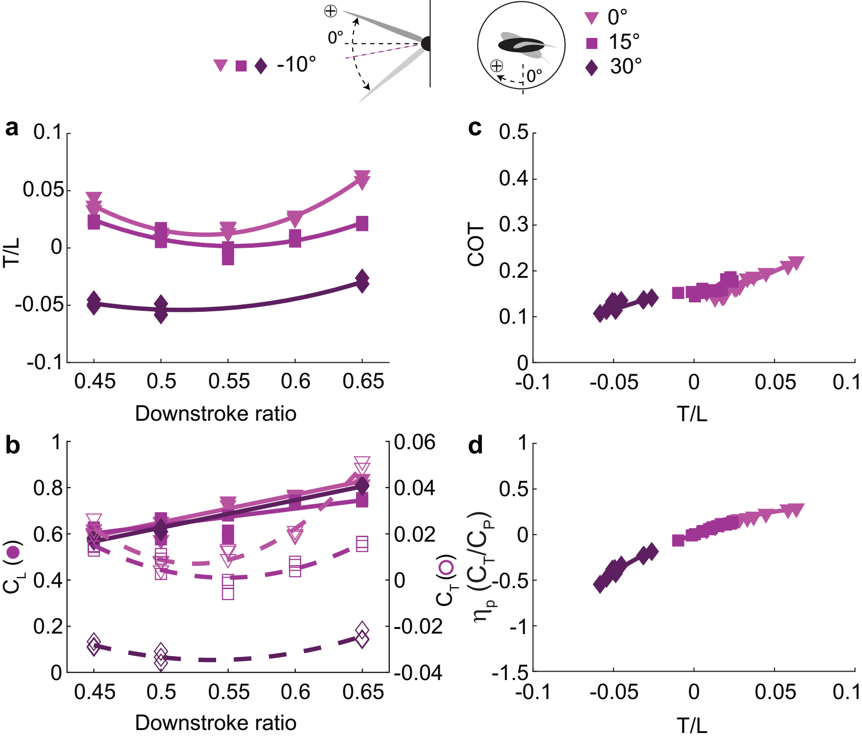
⊕
0°
▼ ■ ◆ -10°
⊕
0°
▼ 0°
■ 15°
◆ 30°
a
T/L
0.1
0.05
0
-0.05
-0.1
0.45
0.5
0.55
0.6
0.65
Downstroke ratio
b
C_L (●)
C_T (○)
1
0.8
0.6
0.4
0.2
0
0.06
0.04
0.02
0
-0.02
-0.04
0.45
0.5
0.55
0.6
0.65
Downstroke ratio
c
COT
0.5
0.4
0.3
0.2
0.1
0
-0.1
-0.05
0
0.05
0.1
T/L
d
η_p (C_T/C_P)
1
0.5
0
-0.5
-1
-1.5
-0.1
-0.05
0
0.05
0.1
T/L

PNAS

Supporting Information for
Aerodynamic efficiency explains flapping strategies used by birds.

L. Christoffer Johansson*

* L. Christoffer Johansson
Email: Christoffer.Johansson@biol.lu.se

This PDF file includes:

- Supporting text
- Supporting references
- Figures S1 to S4

Supporting Text

Material and methods

The statistical models fitted to the data were the following, and all variables were treated as continuous if not stated otherwise.

Fig. 2a, Y(*T*/*L*), Effects(*St*, *f*, *f* * *St*). *f* was treated as ordinal.
Fig. 2c, Y(COT), Effects(*MWE*, *f*, *St*, *St* * *MWE*, *St* * *f*).
Fig. 2d, Y($\mathrm{h_p}$(k=2.8)), Effects(*MWE*, *f*, *St*, *St* * *f*, *St* * *MWE*). *MWE* was treated as nominal.

Fig. 3a, Y(*T*/*L*), Effects(*f*, A_{deg}, *f* * A_{deg}). *f* was treated as ordinal.
Fig. 3b, Y($\mathrm{C_L}$, $\mathrm{C_T}$), Effects(*MWE*).
Fig. 3c, Y(COT), Effects(*Group*, *T*/*L*, *T*/*L* * *Group*), where *Group* refers to the combination of *f* and constant vs changing *MWE*. *Group* was treated as nominal.
Fig. 3d, Y($\mathrm{h_p}$ (k=3.8)), Effects(*T*/*L*, Group, *T*/*L* * *Group*). *Group* was treated as nominal.

Fig. 4a, Y(*T*/*L*), Effects(*dsR*, *SPA*, dsR^2, *dsR* * *SPA*, dsR^2 * *SPA*). *SPA* was treated as nominal.
Fig. 4b, Y($\mathrm{C_L}$), Effects(*SPA*, *dsR*, *dsR* * *SPA*) and Y($\mathrm{C_T}$), Effects(*SPA*, *dsR*, dsR^2, *dsR* * *SPA*, dsR^2 * *SPA*). *SPA* was treated as ordinal.
Fig. 4c, Y(COT), Effects(*dsR*, *SPA*, *T*/*L*). *SPA* was treated as nominal.
Fig. 4d, Y($\mathrm{h_p}$ (k=4.4)), Effects(*T*/*L*, *SPA*, *T*/*L* * *SPA*, *dsR*, *dsR* * *T*/*L*). *SPA* was treated as nominal.
Y($\mathrm{h_p}$ (k=4.4)), Effects(*T*/*L*, *Strategy*, *T*/*L* * *Strategy*), where *Strategy* refers to changing *f* and A_{ang} or *SPA* and *dsr*. *Strategy* was treated as nominal.

Fig. S3a, Y($1/(\mathrm{C_F}^{1.5}/\mathrm{C_P})$), Effects(*Group*, *T*/*L*, *T*/*L* * *Group*). *Group* was treated as nominal.
Fig. S3b, Y($\mathrm{F_{use}}$/e), Effects(*Group*, *T*/*L*, *T*/*L* * *Group*). *Group* was treated as nominal.
Fig. S3c, Y($1/(\mathrm{C_F}^{1.5}/\mathrm{C_P})$), Effects(*St*, *MWE*, *f*, *St* * *MWE*, *St* * *f*). *MWE* was treated as nominal.
Fig. S3d, Y($\mathrm{F_{use}}$/e), Effects(*St*, *MWE*, *f*, *St* * *MWE*, *St* * *f*). *MWE* was treated as nominal.
Fig. S3e, Y($1/(\mathrm{C_F}^{1.5}/\mathrm{C_P})$), Effects(*T*/*L*, *SPA*, *dsR*, *T*/*L* * *SPA*, *T*/*L* * *dsR*).
Fig. S3f, Not tested.

Results and discussion

The results from the $F_{use}/\bar{\varepsilon}$ (where F_{use} is the total useful force and $\bar{\varepsilon}$ is the enstrophy) were not presented in the main text, but to a large extent follow the same patterns as PF, but with relatively more variation in the data. $F_{use}/\bar{\varepsilon}$ decreased with *T/L* (Supplemental Fig. S3b, $p<0.0001$), similar to PF. There was a significant difference between the MWE strategy and the non-MWE strategy in the slope, but only for the data that used the same *f* (Supplemental Fig. S3b, *T*/*L* * Group(4.5 Hz) $p=0.0479$). $F_{use}/\bar{\varepsilon}$ decreased with *St* (Supplemental Fig. S3d, $p<0.0001$), similar to PF, which supported the conclusion that the efficiency of generating F_{use} decreases with increasing *St*, at least within the measurement range. In addition, $F_{use}/\bar{\varepsilon}$ was lower and had lower slopes for the *MWE* strategy compared to the zero-*MWE* strategy when comparing across *St* (Supplemental Fig. S3d, *MWE* $p<0.0001$, *St* * *MWE* $p=0.0090$), following the same trend as PF.

In addition to the main findings, I found a significant interaction effect between A_{ang} and *f* so that *T*/*L* increased faster with A_{ang} at high *f* than at low *f* (Fig. 3a, A_{ang}**f*, $p<0.0001$). This suggests that pitch rate may affect the *T*/*L*, providing an interesting avenue for future research. Pitch rate could influence force production through "fanning", similar to what has been suggested for slow flying bats (1) or through controlling the rotational circulation, which can have an significant effect also in forward flight (2). This interaction effect between A_{ang} and *f* could also be linked to my findings that increased *f* resulted in higher $\mathrm{h_p}$ for a given *St* (Fig. 2d, $p<0.0001$), but also in a higher COT (Fig. 2c, $p<0.0001$) and a larger effect of *f* at higher *St* than at lower (Fig. 2b, *St***f*, $p<0.0001$). Together with my findings that there may be a wing-wing interaction effect also when the wings are relatively far apart this suggests that these effects that are generally ignored in cruising flight need further attention in systems with flapping wings pivoting around their base.

Supporting References

1. L. C. Johansson, J. Håkansson, L. Jakobsen, A. Hedenström, Ear-body lift and a novel thrust generating mechanism revealed by the complex wake of brown long-eared bats (*Plecotus auritus*). *Sci. Rep.* **6**, 24886 (2016).

2. M. Sun, J. H. Wu, Aerodynamic force generation and power requirements in forward flight in a fruit fly with modeled wing motion. *J. Exp. Biol.* **206**, 3065–3083 (2003).

3. E. Ajanic, A. Paolini, C. Coster, D. Floreano, C. Johansson, Robotic avian wing explains aerodynamic advantages of wing folding and stroke tilting in flapping flight. *Adv. Intell. Syst.* **5**, 2200148 (2023).

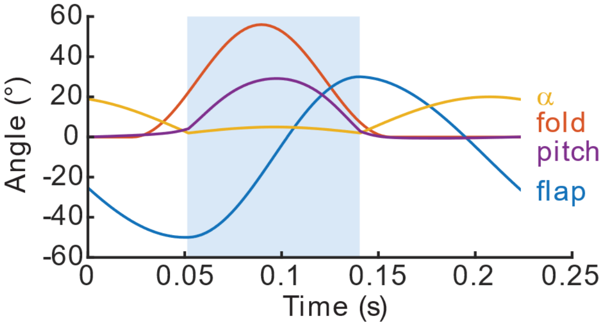

Fig. S1. A sample wingbeat used by the robot. Flapping frequency is 4.5 Hz, flapping amplitude 80 degrees, mean wing elevation -10 degrees and downstroke ratio 0.6. The wing is folded during the upstroke and the angle of attack (α) is set to peak at 20 degrees, mid-span, during the downstroke and at 5 degrees during mid upstroke, while set at 2 degrees at the turning points. The pitch is adjusted to maintain the prescribed α taking the flapping and forward speed into account, resulting in a pitch angle close to zero during the downstroke and a pitch up during the upstroke. Light blue background represents upstroke.

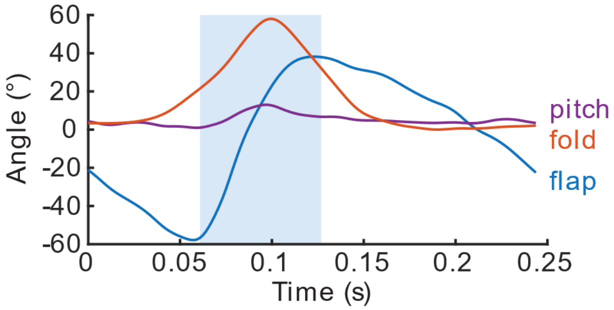

Fig. S2. Kinematic pattern for a single wingbeat of a jackdaw. The bird was flying at 8.7 m/s with a wingbeat frequency of 4.1 Hz. The flapping amplitude was 96 degrees, with a mean wing elevation of -20 degrees and a downstroke ratio of 0.73. The wing was folded during the upstroke and here the curve represents the wing length reduction scaled so that the minimum has the same value as the angular value of Fig. S1. The pitch of the wing is close to zero during the downstroke and is pitched up during the upstroke. The curves should only be seen as confirmation that the general patterns of the kinematics used by the robot (e.g. Fig. S1) is relevant for flapping flight in birds. Light blue background represents upstroke.

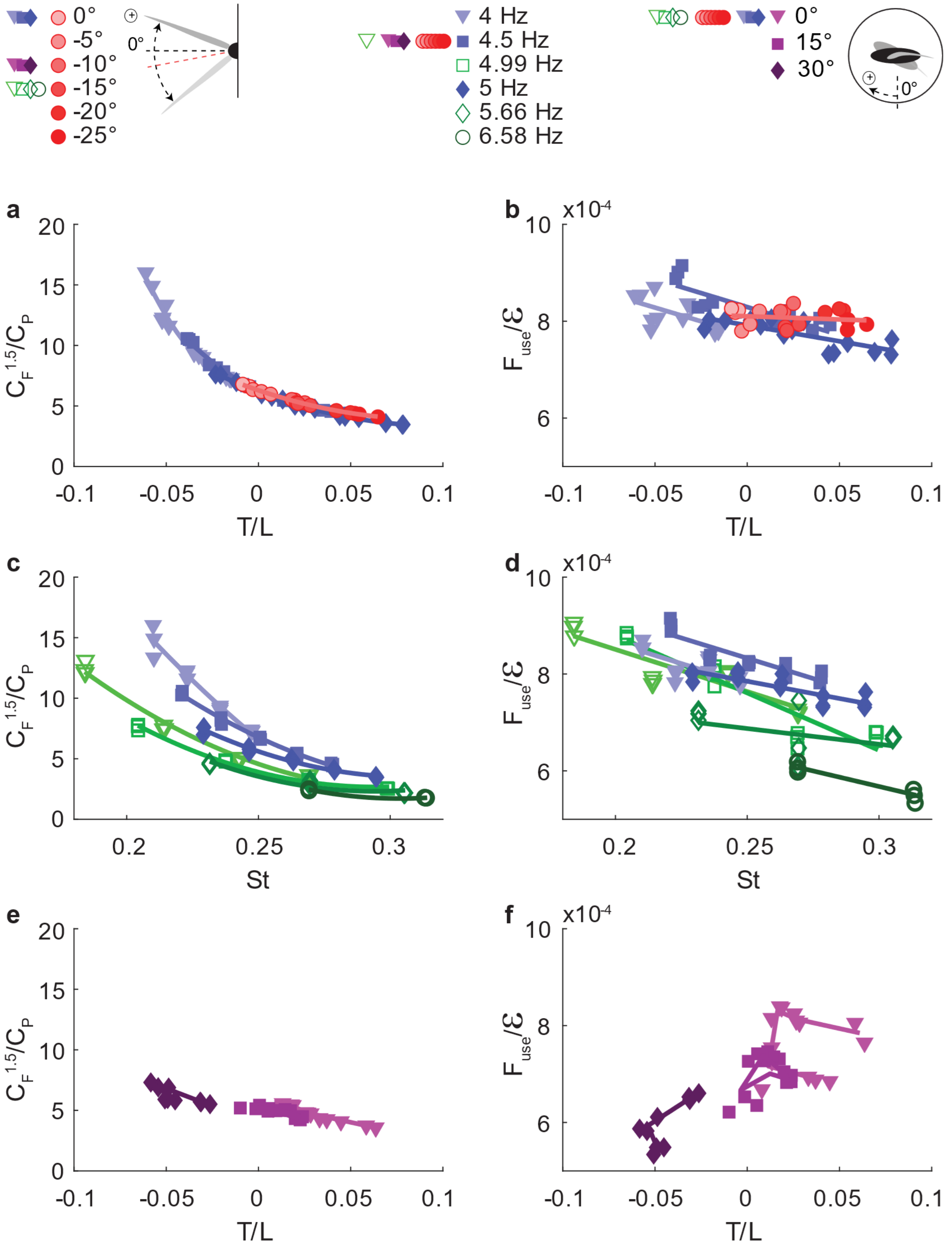

Fig. S3. Alternative measures of efficiency. The power factor ($C_F^{1.5}/C_P$) (a, c, e) and $F_{use}/\bar{\varepsilon}$ (b, d, f) are measures of the "milage" of force generation. Both these factors decrease with increasing *T/L* and Strouhal number (*St*), except for $F_{use}/\bar{\varepsilon}$ when changing stroke plane angle and downstroke ratio (f). The legend shows, from left to right, the mean wing elevation (*MWE*), wingbeat frequency and stroke plane angle (*SPA*). Figure partly adapted from ref. (3), which is licensed under CC BY 4.0.

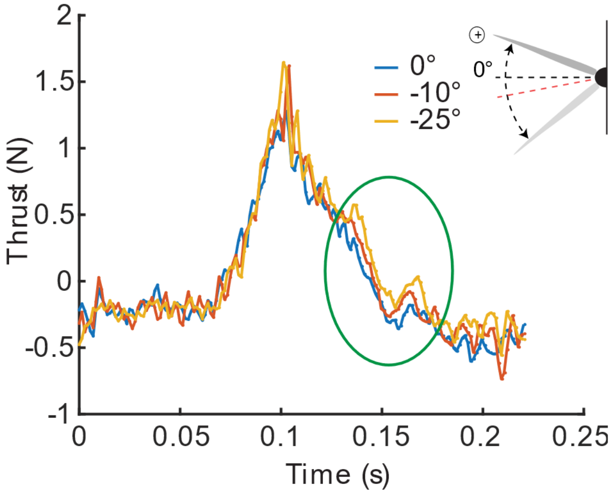

Fig. S4. Thrust during wingbeats with different mean wing elevation (*MWE*). Decreasing the *MWE*, while keeping all other kinematic parameters constant, results in an increase in thrust during the end of the downstroke (encircled in green), indicating the cause is a wing-wing interaction. The curves represent the means of all sequences with the same kinematic parameters. Figure partly adapted from ref. (3), which is licensed under CC BY 4.0.